Journal of Solid State Chemistry **145,** 604–611 (1999)
Article ID jssc.1999.8249, available online at http://www.idealibrary.com on IDEAL®

Studies on Tetragonal $Na_2CoP_2O_7$, a Novel Ionic Conductor

F. Sanz,* C. Parada,† J. M. Rojo,* C. Ruiz-Valero,*,[1] and R. Saez-Puche†

** Instituto de Ciencia de Materiales de Madrid, CSIC, Cantoblanco, E-28049 Madrid, Spain; and †Departamento de Química Inorgánica, Facultad de Ciencias Químicas, Universidad Complutense, E-28040 Madrid, Spain*

Received November 10, 1998; in revised form February 16, 1999; accepted February 26, 1999

Crystals of the tetragonal form of $Na_2CoP_2O_7$ have been grown and characterized by single crystal X-ray diffraction. This compound crystallizes in the tetragonal system, space group $P4_2/mnm$ with $a = 7.7058(12)$, $c = 10.301(2)$ Å, and $Z = 4$. The structure was solved by Patterson and Fourier methods, and refined to final agreement factors $R(F^2) = 5.8\%$, $Rw(F^2) = 12.4\%$, $S(F^2) = 1.07$. Their structure can be described as layered since it is formed by slabs of $[CoP_2O_7]_\infty$ with Na cations lying between the layers. The Co^{2+} cation adopts a tetrahedral coordination geometry unusual in inorganic solids. CoO_4 tetrahedra share four oxygens with P_2O_7 pyrophosphate groups and the Na^+ cations appear in a NaO_8 quadrangular prismatic coordination geometry. Magnetic measurements reveal the presence of antiferromagnetic interactions in the Co^{2+} sublattice, at about 10 K. Magnetic correlations are also studied from the analysis of possible superexchange pathways in the structure. Impedance measurements (frequency range: $1–5 \times 10^6$ Hz; temperature range: 90–540°C) show $Na_2CoP_2O_7$ an ionic conductor being the conductivity at 300°C 2×10^{-5} Scm^{-1} and the activation energy 0.61 eV. The possible motion of the Na^+ ions in the interlayer surface plane and through adjacent layers (c axis) is discussed.

Key Words: **diphosphate; structure; ionic conductor; antiferromagnetic; layered.**

INTRODUCTION

We have recently reported the synthesis and structure of $Na_4M^{II}_3(PO_4)_2(P_2O_7)$ (M = Co) (1) and we have studied the magnetic properties and ionic conductivity of this new family of phosphate material (M = Mn, Co, Ni) (2). The present paper is an extension of our work on mixed diphosphates containing both alkaline and divalent transition metal cations.

In the literature we have found the structure of two forms of $Na_2CoP_2O_7$, one of them is rose colored and triclinic and the other is blue and orthorhombic (3). A third tetragonal form is known from X-ray powder diffraction for $A_2M^{II}P_2O_7$ when A = Na, K and M = Co, Cu, Zn (4, 5), which presents the melilite structure type (6, 7), but there are no structural dates of these because nobody has grown single crystals to solve the structure.

The purpose of the present paper is to report crystal growth and structure of the tetragonal form of $Na_2CoP_2O_7$ in order to contribute to a better insight into the crystal chemistry of the diphosphates $A_2B^{II}P_2O_7$ isolated within the binary diagrams $A^I_4P_2O_7 - B^{II}_2P_2O_7$, where A^I and B^{II} are monovalent and divalent cations, respectively. The tetragonal form seems to be a derivative of the orthorhombic form (3). The framework is a layered structure where the cobalt cation exhibits a tetrahedral coordination that is not very frequent in inorganic solids (8) and interlayer linkages are made via the sodium ions. Although in the past few years many efforts have been made to dope the $AlPO_{4-n}$ family, by substitution for Al^{3+} of Co(II) in a tetrahedral coordination due to their selective redox catalytic properties (9–11), only a few examples of framework structures based on cobalt, phosphorus, and oxygen are described in which cobalt is exclusively in a tetrahedral environment (12–13). The structure is compared here with that of the orthorhombic form and with those of the layered α- and β-$Na_2CuP_2O_7$ (14, 15). We have also investigated the magnetic properties and the ionic conductivity in this layered material, showing antiferromagnetic and ionic conductor behavior.

EXPERIMENTAL

Synthesis

Single crystals of this phosphate were grown by melting a mixture of $NaNO_3$, $Co(CH_3CO_2)\cdot 4H_2O$, and $NH_4H_2PO_4$ in molar ratios 4 : 3 : 4. After grinding, the mixture was heated to 1070 K and cooled at 10°C/h to 873 K. The sample was finally quenched to room temperature. Two types of crystals were extracted from the resulting product, which showed rose and blue colors, respectively. The rose crystals were identified as $Na_4Co_3(PO_4)_2(P_2O_7)$, previously studied by us (1). The blue crystals correspond to the tetragonal form of $Na_2CoP_2O_7$.

[1] To whom correspondence should be addressed.

0022-4596/99 $30.00

We have also obtained the polycrystalline powder of this material for magnetic and ionic conductivity measurements. The bright indigo-colored powder was synthesized according to a previous report (4).

Single Crystal X-Ray Diffraction

A blue-colored crystal of prismatic shape was resin epoxy coated and mounted on a Siemens Smart CCD diffractometer equipped with a normal focus, a 2.4 kW sealed tube X-ray source (Mo$K\alpha$ radiation, $\lambda = 0.71073$ Å), operating at 50 kV and 40 mA. Data were collected over a hemisphere of reciprocal space by a combination of three sets of exposures. Each set had a different φ angle for the crystal and each exposure of 20 s covered 0.3° in ω. The crystal to detector distance was 6.01 cm. Coverage of the unique set was over 99% complete to at least 23° in θ. Unit cell dimensions were determined by a least-squares fit of 50 reflections with $I > 20\sigma(I)$ and $6° < 2\theta < 46°$. The first 30 frames of data were recollected at the end of the data collection to monitor crystal decay. The intensities were corrected for Lorentz and polarization effects. Scattering factors for neutral atoms and anomalous dispersion corrections for Co, Na, and P were taken from "International Tables for X-Ray Crystallography" (16). The structure was solved by Patterson methods and refined in the tetragonal space group $P4_2/mnm$. Full matrix least-squares refinement was carried out by minimizing $w(F_o^2 - F_c^2)^2$. Refinement on F^2 for all reflections, weighted R factors (R_w), and all goodness of fit S are based on F^2, while conventional R factors (R) are based on F; R factors based on F^2 are statistically about twice as large as those based on F, and R factors based on all data will be even larger.

All calculations were performed using SMART software for data collection, SAINT (17) for data reduction; SHELXTL™ to refine the structure and to prepare material for publication (18), and ATOMS (19) for molecular graphics.

Elemental Analysis

Chemical analysis was carried out on an ICP (induced coupling plasma) apparatus. The observed data (16.2% Na, 20.9% Co, and 21.8% P) are in good agreement with the calculated data (16.5% Na, 21.1% Co, and 22.2% P).

X-Ray Powder Diffraction

An X-ray powder pattern was taken at room temperature by using a Siemens D-500 diffractometer in the step scan mode, Cu$K\alpha$ radiation 1.5406 Å, at a step value of 0.02°, measuring for 20 s at each step. The observed reflections were indexed on a tetragonal unit cell (20) in agreement with the parameter obtained from the single crystal X-ray study.

Magnetic Measurements

Magnetic susceptibility was measured using a Quantum Design MPMS-XL Squid magnetometer operating from 300 to 2 K at 500 Oe.

Ionic Conductivity

Impedance measurements were carried out in a frequency response analyzer Solartron 1174 coupled to an electrochemical interface Solartron 1286. The frequency range was 1–10^5 Hz. In some particular cases, when the impedance was lower than $10^6\,\Omega$, an impedance/gain-phase analyzer, Solartron 1260, was used. The frequency range was 5–5×10^6 Hz. Pellets of ca. 9 mm diameter and 1.5 mm thickness were prepared by cold pressing the powder sample at 110 MPa. Then the pellets were sintered at 650°C for 24 h. Platinum electrodes were painted on the two faces of the pellets with a platnium paste (Engelhard 6082); then the painted pellets were heated at 200°C for 2 h and at 650°C for 4 h. The impedance measurements were carried out at steady state temperatures on the pellets in still air.

RESULTS AND DISCUSSION

Crystal Structure

A summary of the fundamental crystal data is given in Table 1. Final atomic coordinates, selected bond distances and angles, and anisotropic thermal parameters are given in Tables 2, 3, and 4, respectively.

A view of the structure along the [100] direction is shown in Fig. 1, from which the layer-like nature is really apparent with the sodium ions located between the layers. Figure 2 shows a plan view of one of the layers along the [001] direction. Each layer consists of CoO_4 isolated tetrahedra interconnected by bridging P_2O_7 groups through the O2 oxygen atom, forming five member rings in continuous sheets in the *ab* plane. The Na cations are located above and below the pentagonal rings. The overall structure consists of $[CoP_2O_7]_\infty^{2-}$ layers in which the sodium cations are embedded. Therefore, the structural role of Na^+ cations is only to maintain the charge neutrality and to prevent the layers from bending or collapsing.

The cobalt atom, located at the special position (4d) with point symmetry 4, has tetrahedral coordination to the O2 oxygen atoms of the diphosphate group. According to the four site symmetry of the Co atom, the CoO_4 tetrahedra are aligned parallel to the c axis and may only be distorted by an elongation or compression along this axis. However, the CoO_4 tetrahedron is very regular, as is shown in Table 3, and the Co–O distance is in agreement with crystal chemistry expectations (8).

The diphosphate group, P_2O_7, is formed as usual by two PO_4 tetrahedra which share the oxygen atom O3. This

TABLE 1
Crystal Data and Structure Refinement for $Na_2CoP_2O_7$

Empirical formula	$Na_4Co_2P_4O_{14}$
Formula weight	557.70
Temperature	295(2) K
Wavelength	0.71073 Å
Crystal system	Tetragonal
Space group	$p4_2/mnm$
Unit cell dimensions	$a = 7.7058(12)$ Å, alpha = 90°
	$b = 7.7058(12)$ Å, beta = 90°
	$c = 10.301(2)$ Å, gamma = 90°
Volume,z	611.6(2) Å^3, 2
Density (calculated)	3.028 Mg/m^3
Absorption coefficient	3.459 mm^{-1}
$F(000)$	540
Crystal size	0.02 × 0.04 × 0.2 mm
Θ range for data collection	3.30 to 23.23°
Limiting indices	$-6 \le h \le 7,\ -8 \le k \le 7,\ -4 \le l \le 11$
Reflections collected	1194
Independent reflections	262 ($R_{int} = 0.1084$)
Absorption correction	None
Refinement method	Full-matrix least-squares on F^2
Data/restraints/parameters	262/0/36
Goodness-of-fit on F^2	1.071
Final R indices [$I > 2\sigma(I)$]	$R1 = 0.0581$, w$R2 = 0.1247$
R indices (all data)	$R1 = 0.0876$, w$R2 = 0.1357$
Largest diff. peak and hole	0.569 and −0.691 e Å^{-3}

TABLE 3
Selected Bond Lengths [Å] and Angles [°] for $Na_2CoP_2O_7$

Co(1)–O(2)^a	1.956(6)	Co(1)–O(2)^b	1.956(6)
Co(1)–O(2)	1.956(6)	Co(1)–O(2)^c	1.956(6)
P(1)–O(1)	1.484(8)	P(1)–O(2)	1.496(6)
P(1)–O(2)^d	1.496(8)	P(1)–O(3)	1.582(6)
Na(1)–O(1)^e	2.615(8)	Na(1)–O(1)^f	2.615(8)
Na(1)–O(1)^g	2.615(8)	Na(1)–O(1)^b	2.615(8)
Na(1)–O(2)^d	2.668(8)	Na(1)–O(2)^h	2.668(8)
Na(1)–O(2)	2.668(8)	Na(1)–O(2)^i	2.668(8)
Na(1)–Na(1)^j	3.11(2)	Na(1)–Na(2)^g	3.645(7)
Na(2)–O(1)^k	2.347(10)	Na(2)–O(1)	2.347(10)
Na(2)–O(3)^b	2.695(10)	Na(2)–O(3)^l	2.695(10)
Na(2)–O(2)^b	2.735(8)	Na(2)–O(2)^m	2.735(8)
Na(2)–O(2)^n	2.735(8)	Na(2)–O(2)^o	2.735(8)
O(2)^a–Co(1)–O(2)^b	106.8(2)	O(2)^a–Co(1)–O(2)	114.9(4)
O(2)^b–Co(1)–O(2)	106.8(2)	O(2)^a–Co(1)–O(2)^c	106.8(2)
O(2)^b–Co(1)–O(2)^c	114.9(4)	O(2)–Co(1)–O(2)^c	106.8(2)
O(1)–P(1)–O(2)	115.8(3)	O(1)–P(1)–O(2)^d	115.8(3)
O(2)–P(1)–O(2)^d	108.1(6)	O(1)–P(1)–(3)	110.6(6)
O(2)–P(1)–O(3)	102.4(4)	O(2)^d–P(1)–(3)	102.4(4)

Note. Symmetry transformations used to generate equivalent atoms: $^a -x+1, -y, z$; $^b y+1/2, -x+1/2, -z+1/2$; $^c -y+1/2, x-1/2, -z+1/2$; $^d -y+1, -x+1, z$; $^e -y+3/2, x-1/2, -z+1/2$; $^f y+1/2, -x+1/2, z-1/2$; $^g -y+3/2, x-1/2, z-1/2$; $^h x, y, -z$; $^i -y+1, -x+1, -z$; $^j -x+2, -y, -z$; $^k x, y, -z+1$; $^l -y+3/2, x-1/2, z+1/2$; $^m x+1/2, -y+1/2, z+1/2$; $^n y+1/2, -x+1/2, z+1/2$; $^o x+1/2, -y+1/2, -z+1/2$.

oxygen is located on a binary axis and then generates a twofold internal symmetry for the P_2O_7 group. The plane containing the two phosphorus atoms and the bridging oxygen O3 is parallel to the *ab* plane. The P–O3–P bridge angle is 139.0(10)°, which is in the range of those found in diphosphates reported so far (21). Interatomic distances (Table 3) are similar to those usually observed in previously reported diphosphates (22): one long P–O3 distance (1.582(6) Å) corresponding to a bridging oxygen and three shorter distances almost equal (one O1 = 1.484(8) Å and two O2 = 1.496(6) Å), corresponding to the remaining oxygen atoms of the PO_4 group. The shortest bond (O1) corresponds to unshared oxygen and points into the interlayer space, belonging to the Na atoms coordination environment (Table 3).

TABLE 2
Atomic Coordinates [×10^4] and Equivalent Isotropic Displacement Parameters [Å×10^3] for $Na_2CoP_2O_7$. U(eq) is Defined as One Third of the trace of the Orthogonalized U_{ij} Tensor

	x	y	z	U(eq)
Co(1)	5000	0	2500	29(1)
P(1)	6359(3)	3641(3)	2113(3)	28(1)
Na(1)	8574(7)	1426(7)	0	38(2)
Na(2)	8026(7)	1974(7)	5000	39(2)
O(1)	6362(7)	3638(7)	3554(8)	38(2)
O(2)	5786(10)	1990(8)	1478(6)	70(3)
O(3)	5000	5000	1575(14)	110(8)

The tetragonal structure of $Na_2CoP_2O_7$ belongs to the melilite type (6, 7). Melilite forms a pseudobinary solid solution between the members akermanite (23), $Ca_2MgSi_2O_7$, and gehlenite (24), $Ca_2Al_2SiO_7$. The magnesium and silicon atoms are distributed into the T(1) and T(2) sites of akermanite (23), respectively, being Mg cation tetrahedrally coordinated, which is rare in silicates. In our case T(1) corresponds to the cobalt site and T(2) to the phosphorus site. Table 5 shows the cell parameters and average distances for $Ca_2Co(Si_2O_7)$ melilite (6, 7) and for the orthorhombic (3) tetragonal forms of $Na_2CoP_2O_7$. It can be observed that in the diphosphates the *c* parameters are double that of silicates.

If now we compare this structure with the others described forms of $Na_2CoP_2O_7$, we can conclude that the tetragonal and triclinic forms have very different structures. While the tetragonal form is layered, the triclinic form has a three-dimensional framework, composed of alternate octahedral cobalt and tetrahedral phosphates arranged in staggered fashion and creating tunnels where sodium atoms are located.

On the other hand, when we compare the structure of the orthorhombic and tetragonal forms (Fig. 3) the same

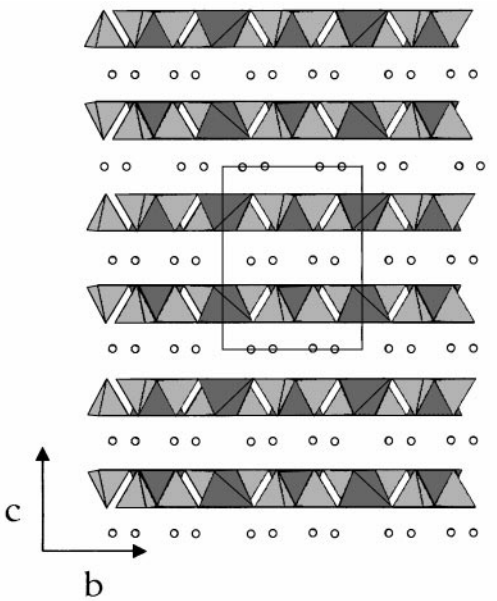

FIG. 1. View of the tetragonal $Na_2CoP_2O_7$ structure along [100], showing the layered nature. The Na^+ cations are represented by open circles.

$[CoP_2O_7]_\infty^{2-}$ sheets can be observed. Table 5 shows that the *c* parameter in the orthorhombic phase is double the *a* parameter in the tetragonal phase, and the *R* value in the orthorhombic phase is too high. All of this allows us to discuss whether these forms are identical or different. In both cases, the Co cation shows a tetrahedral coordination with Co–O average bond lenghts 1.956(6) and 1.95(2) Å for tetragonal and orthorhombic phases, respectively. The diphosphate group exhibits in eclipse and quasi-eclipse

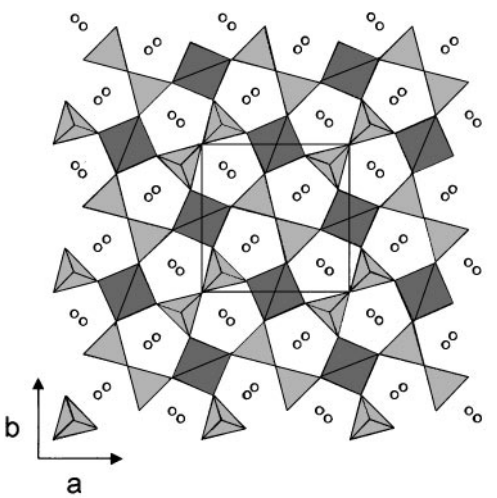

FIG. 2. View of the tetragonal $Na_2CoP_2O_7$ structure along [001], showing the five member rings.

TABLE 4
Anisotropic Thermal Parameters [$Å^2 \times 10^3$] for $Na_2CoP_2O_7$. The Anisotropic Displacement Factor Exponent Takes the Form: $-2\pi^2[(ha^*)^2U_{11} + \ldots + 2hka^*b^*U_{12}]$

	*U*11	*U*22	*U*33	*U*23	*U*13	*U*12
Co(1)	30(1)	30(1)	27(1)	0	0	0
P(1)	22(2)	22(2)	42(2)	−1(1)	1(1)	10(2)
Na(1)	33(3)	33(3)	48(4)	0	0	5(4)
Na(2)	40(4)	40(4)	38(4)	0	0	16(4)
O(1)	32(4)	32(4)	48(5)	0(3)	0(3)	19(5)
O(2)	128(8)	33(5)	48(4)	−3(3)	8(4)	−45(5)
O(3)	144(13)	144(13)	43(9)	0	0	134(16)

forms with average $P–O_{terminal}$ distances of 1.492(6) and 1.50(2) Å and $P–O_{bridging}$ distances 1.582(6) and 1.61(2) Å for tetragonal and orthorhombic forms, respectively. The Na atoms are in both cases eight coordinate with average distances 2.64(2) Å for the orthorhombic phase and 2.634(8) Å for the tetragonal phase. Consequently, there is not a significant difference between orthorhombic and tetragonal structures. In fact, we have refined the crystal structure in the orthorhombic system by doubling the *c* parameter, obtaining the same results as those reported in the literature (3): an *R* value ≈ 10 and only isotropic refinement could be performed.

As can be seen in Table 4, in the tetragonal phase all the anisotropic thermal parameter determinants were positive whereas in the orthorhombic phase several of them became negative and the standard deviations were larger. The O3 atom, which is situated in a special position in the tetragonal cell, has a higher temperature factor than the other oxygen atoms, which can be attributed to a minor positional disorder around this site. This disorder is not large enough to force the refinement in the orthorhombic double cell. Therefore, we can conclude that, at the moment, there are only two forms of $Na_2CoP_2O_7$: one of them rose colored, triclinic, with a tridimensional framework and another blue colored, tetragonal, with a layered structure.

From another point of view, we can compare also the tetragonal $Na_2CoP_2O_7$ with the two known layered structures of α- and β-$Na_2CuP_2O_7$ and we find some similarities and significant differences. The three structures are composed of infinite layers $[MP_2O_7]_n^{2n-}$ made of alternating diphosphate groups $(P_2O_7)^{4-}$ and M^{2+} cations. The principal differences between tetragonal $Na_2CoP_2O_7$ and the α- and β-$Na_2CuP_2O_7$ forms reside in shape of the layers, the *M*(II) polyhedron coordination, and the way the sodium cations are set out between appropriate layers. The α-$Na_2CuP_2O_7$ is formed by pairs of $[MP_2O_7]_n^{2n-}$ flat ribbons symmetrically related by a center of inversion and a glide plane *n*. The Cu atoms exhibit a square-pyramidal coordination, and the Na^+ cations are located in two different

TABLE 5
Crystallographic Data for Cobalt Silicates and Phosphates with Melilite Structure Type

Compound	a(Å)	b(Å)	c(Å)	V(Å^3)	Space group	R%	⟨Co–O⟩Å	⟨Si/P–O⟩Å	Ref.
$Ca_2Co(Si_2O_7)$	7.8258(4)		5.0148(5)	307.12	$P\text{-}42_1m$	4.5	1.9263(5)	1.608(6)	6
$Ca_2Co(Si_2O_7)$	7.8417(6)		5.0249(3)	308.99	$P\text{-}42_1m$	4.8	1.9397(6)	1.618(8)	7
$Na_2Co(P_2O_7)$	7.713(2)	15.378(6)	10.271(4)	1218.2(8)	$P2_1cn$	9.9	1.95(2)	1.53(2)	3
		c	b						
$Na_2Co(P_2O_7)$	7.706(1)		10.301(2)	611.6(2)	$P4_2/mnm$	5.8	1.956(6)	1.515(6)	[a]

Note. In Ref. (3) parameters b and c have been interchanged for a better comparison.
[a] Present paper.

sites corresponding to a coordination number of 8 for Na1 and 6 for Na2 with a mean value Na–O of 2.559 Å for Na1 and 2.500 Å for Na2. In β-$Na_2CuP_2O_7$ all the ribbons $[MP_2O_7]_n^{2n-}$ are corrugated, the Cu atoms are in a planar square coordination, and all sodium atoms are six-coordinated with a mean value Na–O of 2.424 Å. The title compound is formed by flat layers, the Co atom adopts a tetrahedral coordination, and the Na^+ cations appear in a NaO_8 quadrangular prism coordination with a mean bond length of 2.641(8) Å for Na1 and 2.628(9) Å for Na2.

Magnetic Properties

Figure 4 shows the variation of the reciprocal molar susceptibility with the temperature for $Na_2CoP_2O_7$. It can be observed that the susceptibility obeys a Curie–Weiss law over a wide temperature range, between 300 and 10 K, and the calculated magnetic moment takes the value of 4.40 B.M. which agrees with those obtained for other tetrahedral Co(II) compounds (25).

The upward deviations from the Curie–Weiss behavior below 10 K can be due to two different reasons (26). First, this deviation can be attributed to the depopulation of the higher energy level associated to the $^4A_2$ ground state giving rise to a decrease in the susceptibility values and also to the onset of antiferromagnetic interactions in the Co^{2+} sublattice of this material. Both effects appear to be present in our case but the zero field splitting (ZFS) is less important since the Néel temperature estimated from the maximum in the χ vs T plot is 10 K (Fig. 4).

Néel temperature values for other tetrahedral cobalt systems are around 5 K; the higher value of 10 K in our case

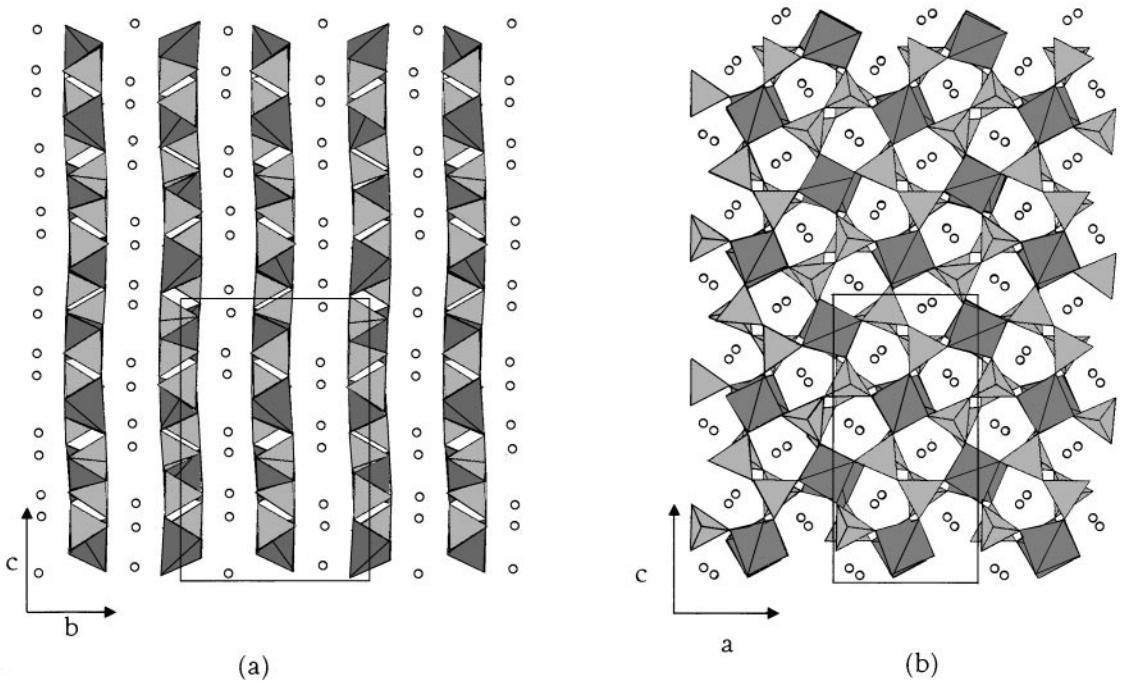

FIG. 3. View of orthorhombic $Na_2CoP_2O_7$ form: (a) along [100], (b) along [010].

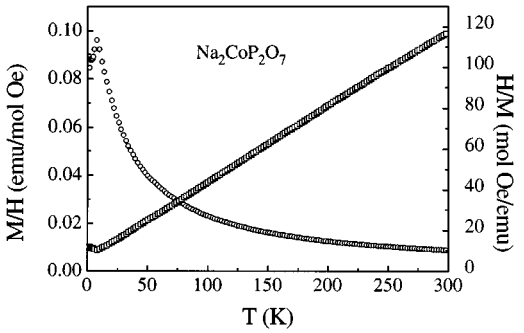

FIG. 4. Magnetic susceptibility (M/H, open circles) and inverse magnetic susceptibility (H/M, open squares) plotted as a function of temperature for $Na_2CoP_2O_7$. $\theta = -19$ K.

can be explained by the previously mentioned antiferromagnetic interactions. To our knowledge, the Néel temperature of 10 K estimated for this compound is the highest reported to date for a tetrahedral Co(II) system (27).

It is worthwhile to give an explanation of these antiferromagnetic interactions, taking into account the possible pathway through which the interactions can take place.

As it can be observed in Fig. 2, the CoO_4 tetrahedral groups are connected by PO_4 groups of the diphosphate P_2O_7 units in the *ab* plane. Therefore, the magnetic behavior can be explained as a consequence of the superexchange interactions Co^{2+}–O–O–Co^{2+} with bond angles quite away from 180° for which the overlapping between the cobalt and oxygen orbitals will decrease.

Consequently, the Néel temperature of 10 K obtained for this compound is fully justified, although each Co(II) cation is surrounded by four Co(II) cations as near neighbors.

Ionic Conductivity

The impedance plots (imaginary vs real part) recorded at two temperatures are shown in Fig. 5a. At low temperatures (180°C) an arc is observed. At higher temperatures (330°C) the arc disappears from the plot and an inclined spike is developed. The presence of the spike is indicative of an ionic conductor that in our compound $Na_2CoP_2O_7$ is ascribed to blocking Na^+ ions at the electrode surfaces. The arc shows a capacitance of 11 pF, which is close to that usually found for grain-interior response, i.e., for the motion of ions within the grains. However, we cannot rule out some grain-boundary contribution in the impedance arc. To ascertain whether the grain-boundary response had a significant contribution to the overall response of the pellets, the electric modulus was analyzed. This parameter, whose imaginary part is related to the impedance through the expression $M'' \propto fZ'$, f being the frequency and Z' the real impedance, is chosen because it gives information of the grain-interior response but is not affected by the grain-boundary one (28–30). M'' vs

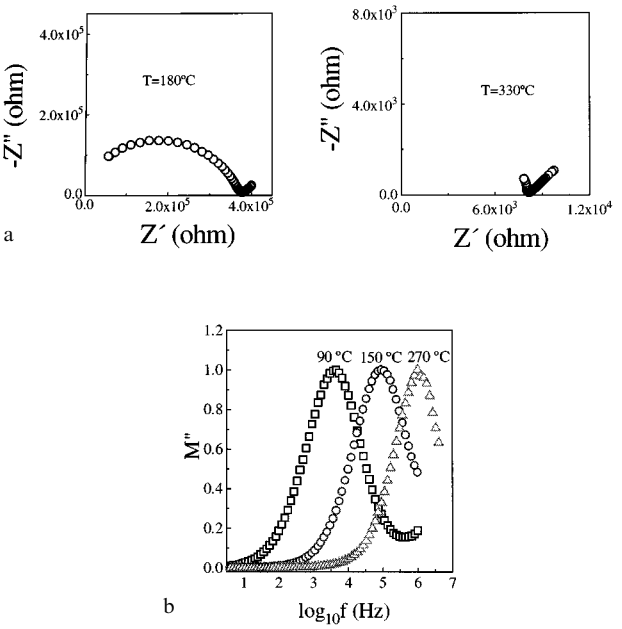

FIG. 5. (a) Impedance plots (imaginary $-Z''$ vs real Z') obtained at two temperature for the $Na_2CoP_2O_7$ pellet. (b) Normalized imaginary modulus vs frequency in a semi-log scale at three temperatures.

frequency in a semilog scale is plotted in Fig. 5b. An asymmetric peak is observed which shifts toward higher frequency at increasing temperatures. The frequency at the maximum of the peak was measured at different temperatures and the values were represented in an Arrhenius plot in Fig. 6. In this figure the ionic conductivity reduced from the impedance arcs is also represented. The overall resistance of the arcs was estimated from the intercept of the low-frequency end of the arcs or of the spike with the real Z' axis. Then, the overall conductivity was calculated

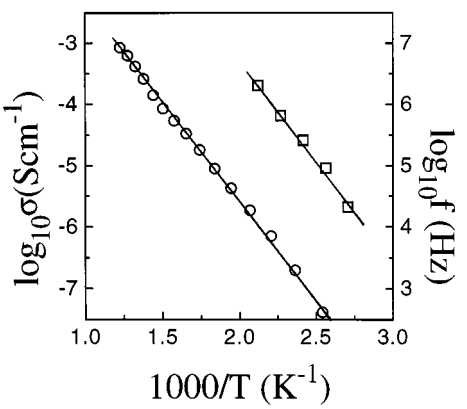

FIG. 6. Plots of the conductivity (circles) and frequency of the modulus peak (squares) vs inverse temperature. The straight lines are best fits to the expressions $\sigma = \sigma_0 \exp(-E_\sigma/kT)$ and $f = f_0 \exp(-E_f/kT)$.

TABLE 6
Activation Energies (E_σ and E_f) and Pre-Exponential Factors (σ_0 and f_0) for the Arrhenius Plots of Fig. 6. Conductivity at 300°C Is Also Included

Sample	E_σ (eV)	σ_0 (Scm^{-1})	E_f (eV)	f_0 (Hz)	$\sigma_{300°C}$ (Scm^{-1})
$Na_2CoP_2O_7$	0.63	6.5	0.61	1.3×10^{12}	2×10^{-5}

as usual. The conductivity and frequency data are well fitted to the expressions $\sigma = \sigma_0 \exp(-E_\sigma/kT)$ and $f = f_0 \exp(-E_f/kT)$, respectively, where σ_0 and f_0 are pre-exponential factors, and E_σ and E_f are activation energies. The activation energies (Table 6) are coincident within experimental error (0.61 eV) indicating that the conductivity deduced from the impedance arcs is dominated by the grain-interior conductivity, i.e., by the motion of the Na^+ ions in the structure.

The framework of a layer and the position of the two crystallographically different Na^+ ions placed above and below the layer are shown in Fig. 7a. The Na(1), represented by closed circles, is surrounded by five nearest neighbor sodiums: four of them are Na(2) and one is Na(1); Na(2), represented by open circles, is also surrounded by five nearest neighbor sodiums: four are Na(1) and one is Na(2). Thus, each sodium could move to five different positions in the interlayer surface.The anisotropic displacement parameters for the two types of sodium in the *a*, *b*, and *c* directions (Table 4) are quite similar. For each sodium they show the same value along the *a* and *b* directions in agreement with the tetragonal symmetry. Along the *c* direction the high anisotropic parameters seem to be related to the presence of big pentagonal holes in the layer. The distance of the two types of sodium to each neighbor in the *ab* plane are marked in Fig. 7b. Two distances of 3.645 and 4.449 Å, between adjacent sites, are observed; the second distance being longer than the first one and, hence, presumably operating as the bottleneck of the motion. Along the *a* and *b* directions Na(1) and Na(2) are arranged in an alternating way; hence the motion of Na^+ ions should occur by hopping between both sites. Regarding the possibility of motion along the *c* axis, the distance of 5.185(3) Å between Na(1) and Na(2) belonging to two adjacent interlayers is slightly longer than the distances found within the interlayer; however, the presence of pentagonal rings in the layers of sufficient size (5.33 Å), as compared with the Na^+ ion diameter (2.32 Å for Na1 and Na2 with a coordination number of 8) (31), could allow the motion through the layers. The lack of single crystals of sufficient size prevented us making electrical measurements along the mentioned directions and, hence, setting up in an unambiguous way the preferential direction for the Na^+ motion.

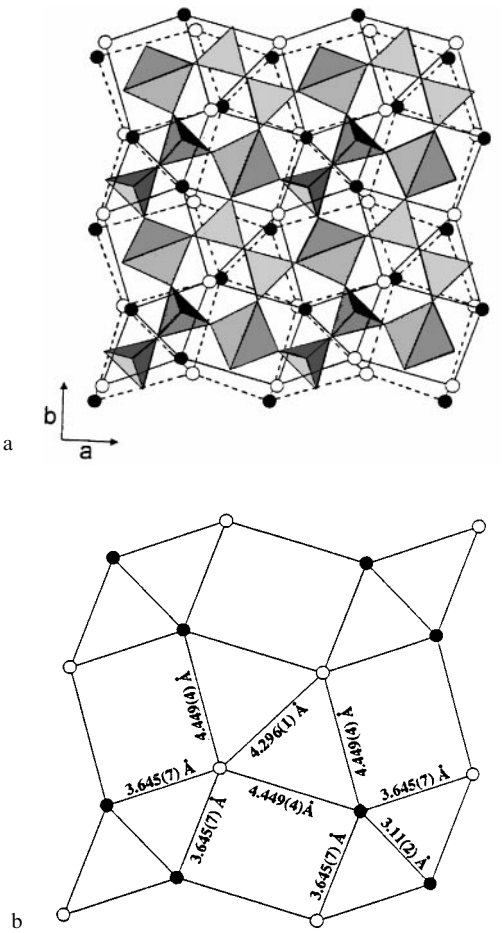

FIG. 7. (a) View of the layer along the *c* direction, showing two adjacent interlayer spaces and the two crystallographically different Na^+ cations. (b) Interlayer sodium cations showing the distances between each Na^+ and nearest neighbors.

ACKNOWLEDGMENTS

This work was supported by the Spanish CICYT under Projects PB94-0031 and MAT 95-0809. We thank the staff of C.A.I. de Espectroscopia de Plasma, Universidad Complutense de Madrid, for chemical analysis and Dr. M. A. Monge and Prof. I. Rasines from ICMM for fruitful comments and discussions.

REFERENCES

1. F. Sanz, C. Parada, U. Amador, M. A. Monge, and C. Ruiz-Valero, *J. Solid State Chem.* **123,** 129 (1996).
2. F. Sanz, C. Parada, J. M. Rojo, and C. Ruiz-Valero, to be published.
3. F. Erragh, A. Boukhari, B. Elouadi, and E. M. Holt, *J. Cryst. Spectrosc.* **21,** 321 (1991).
4. M. Gabelica-Robert, *C. R. Acad. Sc. Paris.* **293,** 497 (1981).
5. J. Majling, S. Palco, F. Hanic, and J. Petrovic, *Chem. Zvesti.* **28,** 294 (1972).
6. M. Kimata, *Neues Jahr. Miner.* **146,** 221 (1983).
7. K. Hagiya, M. Ohmasa, and K. Iishi, *Acta Crystallogr. B* **49,** 172 (1993).

8. M. Wildner, *Z. Kristallogr.* **205,** 51 (1992).
9. C. Montes, M. E. Davis, B. Murray, and M. J. Narayana, *J. Phys. Chem.* **94,** 6425 (1990).
10. L. L. Lin and H. S. Weng, *Appl. Catal. A* **105,** 289 (1993).
11. J. Dakko, and R. A. Sheldon, The Netherlands Patent 9.200.968, 1992.
12. J. Chen, R. H. Jones, S. Natarajan, M. B. Hursthouse, and J. M. Thomas, *Angew. Chem. Int. Ed. Engl.* **33,** 639 (1994).
13. P. Feng, X. Bu, S. T. Tolbert, and G. D. Stucky, *J. Am. Chem. Soc.* **119,** 2497 (1997).
14. K. M. S. Etheredge and S.-J. Hwu, *Inorg. Chem.* **34,** 1495 (1995).
15. F. Erragh, A. Boukhari, F. Abraham, and B. Elouadi, *J. Solid State Chem.* **23,** 120 (1995).
16. "International Tables for X-Ray Crystallography" Vol. IV, p. 72. Kynoch Press. Birmingham, UK, 1974.
17. Siemens, "SAINT, Data Collection and Procedure. Software for the SMART System." Siemens Analytical X-Ray Instruments, Inc., Madison, WI, 1995.
18. Siemens, "SHELEXTL, Version 5.0". Siemens Analytical X-ray Instruments, Inc., Madison, WI, 1995.
19. E. Dowty, "ATOMS for Windows 3.1. A Computer Program for Displaying Atomic Structure." 521 Hidden Valley Road. Kingsport, TN, 1995.
20. P. E. Werner, Univ. of Stockholm, S-106, 91. Stockholm. Sweden, 1984.
21. A. Par, J. Larbot, J. Durand, S. Vilminot, and A. Norbert, *Acta Crystallogr. B* **37,** 1023 (1981).
22. J. J. Chen and K. H. Lii, *J. Solid State Chem.* **76,** 204 (1988).
23. M. Kimata and N. Lii, *Neues Johr. Mineralog.* **1,** 1950 (1981).
24. M. Kimata, M. Shimizu, and S. Saito, *Trans. Am. Cryst. Assoc.* **27,** 301 (1991).
25. R. L. Carlin, "Magneto Chemistry." Springer-Verlag, New York, 1986.
26. M. C. Moron, F. Palacio, J. Pons, J. Casabo, J. and R. L. Carlin, *Eur. J. Solid State Inorg. Chem.* **t28,** 431 (1991).
27. J. Chen, R. H. Jones, S. Natarajam, M. B. Hursthouse, and J. M. Thomas, *Angew. Chem. Int. Ed. Eng.* **33,** 639 (1994).
28. P. B. Macedo, C. T. Moynihan, and R. Bose, *Phys. Chem. Glasses.* **13,** 171 (1972).
29. Y. Hodge, M. D. Ingram, and R. A. West, *Electroanal. Chem.* **74,** 125 (1976).
30. A. Doi, *Solid State Ionics* **31,** 227 (1988).
31. R. D. Shannon, *Acta Crystallogr. A* **32,** 751 (1976).